Applied Surface Science 657 (2024) 159753

Contents lists available at ScienceDirect

Applied Surface Science

journal homepage: www.elsevier.com/locate/apsusc

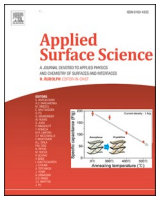

Full Length Article

Thermal annealing induced graphite/diamond structure processed by high-voltage hydroxide ion treatments

F.N. Li [a], P.C. Zhang [b], P.F. Zhang [a,*], H.X. Wang [a,*]

[a] Institute of Wide Band Gap Semiconductors, Xi'an Jiaotong University, Xi'an, China
[b] State Key Laboratory for Mechanical Behavior of Materials, Xi'an Jiaotong University, Xi'an, China

ARTICLE INFO

Keywords:
Diamond
Graphite
Surface treatment
High voltage electrolysis
Ohmic contact

ABSTRACT

Ohmic contacts with low specific contact resistance are necessary for fabrication of diamond electronic devices. This work reports that graphite/diamond ohmic contacts can be obtained by thermal annealing of diamond, patterned by hydroxide ion treatment. Surface graphitization of diamond is achieved through rapid thermal annealing at 1050 °C in vacuum. The thickness of graphite layer is found to be dependent on the duration of annealing with an approximate rate of 3.3 ~ 3.6 nm/minute. The alteration in surface structure is analyzed using Raman spectra, showing a continuously enhanced G peak with increasing annealing time. Early stages of graphitization are discovered by X-ray photoelectron spectroscopy, after annealing diamond samples for merely 0.5 ~ 2 min. Additionally, a distinct atomic interface between graphite and diamond is observed via cross-sectional transmission electron microscopy. Further, the surface graphite is selectively etched by hydroxide ion treatments, protected by gold patterns. In the end, the specific contact resistance of the graphite/diamond contact is determined to be 2.53 × 10^{-4} Ω cm^2 employing the transmission line model.

1. Introduction

Diamond is the "Mount Everest" of electronic and photonic materials with extraordinary properties, such as, wide band gap energy (5.47 eV), high electric breakdown field (10 MV cm^{-1}), high carrier mobility (4500 cm^2 V^{-1} s^{-1} and 3800 cm^2 V^{-1} s^{-1} for electrons and holes, respectively), and high thermal conductivity (2200 W m^{-1} K^{-1}) [1]. Therefore, diamond is considered to be an ultimate semiconductor material for high-power and high-frequency applications, such as metal–oxide–semiconductor field-effect transistors (MOSFETs).

The realization of high output power diamond MOSFETs requires reliable and stable electrode contacts to operate at high temperatures. Particularly, it is necessary to develop ohmic contacts with low specific contact resistance for the source and drain electrodes, so as to increase output power and reduce energy dissipation [2]. Due to wide band gap energy, the formation of ohmic contacts for diamond is mainly fabricated by refractory metals, such as titanium, molybdenum, tungsten, and tantalum. However, refractory metals afford high resistance to thermal and environmental stresses [3].

Recently, a phase engineering concept of 2D materials is developed to greatly improve device performance. The semiconducting phase is used as active channel material, while the phase-engineered metallic phase is used as source/drain electrodes to reduce specific contact resistance [4–6]. The excellent results suggest that phase engineering may be a feasible strategy for diamond devices.

Diamond is composed of sp^3-hybridized carbon atoms, whereas graphite is composed of sp^2-hybridized carbon atoms. Compared to diamond, which has an ultrawide bandgap, graphite is a highly conductive material with a zero bandgap. Diamond devices with laser induced surface graphitization has been reported, exhibiting superior performance [7,8]. However, it is difficult to fabricate sophisticated and micron-sized patterns by laser writing, limited by the mask.

Surface graphitization has been observed by annealing diamond at high temperatures up to 1350 °C in vacuum or 1500 °C in H_2/Ar atmosphere [9–11]. Therefore, graphite/diamond contacts can be achieved by thermal annealing of diamond, which may show low specific contact resistance. However, the electrical properties of the graphite/diamond structure need to be verified. Moreover, the structural transformation of diamond after thermal annealing is to be further investigated.

Based on thermal annealing, the entire surface of diamond is covered by graphite. Moreover, graphite has very good chemical stability,

* Corresponding authors.
E-mail addresses: pfzhang.kk@xjtu.edu.cn (P.F. Zhang), hxwangcn@mail.xjtu.edu.cn (H.X. Wang).

https://doi.org/10.1016/j.apsusc.2024.159753
Received 9 October 2023; Received in revised form 3 February 2024; Accepted 21 February 2024
Available online 22 February 2024

making it difficult for selective corrosion. In order to pattern graphite/diamond contacts for device fabrication, dry etching technique such as inductively coupled plasma is a possible method. However, damage such as lattice distortions of diamond will be induced in the dry etching process [12]. Recently, hydroxide ion treatment of diamond in deionized water at high voltages is developed [13]. It provides a new method for selective corrosion of surface graphite.

In this work, graphite/diamond structure is formed by rapid thermal annealing at 1050 °C in vacuum. The G peak of graphite emerges in Raman spectra after annealing of 5 min, indicating of surface graphitization. However, X-ray photoelectron spectroscopy (XPS) exhibits that surface graphitization already occurs after annealing of 30 s. The cross-sectional transmission electron microscopy (TEM) shows that diamond transforms to nanocrystalline graphite with a distinct interface. Then, the surface graphite is processed by hydroxide ion treatment. In the end, the specific contact resistance of 2.53 × 10^{-4} Ω cm^2 of the graphite/diamond structure was obtained by transmission line model.

2. Material and methods

2.1. Thermal annealing

Chemical vapor deposition (CVD) diamond (1 0 0) substrates (3 × 3 × 0.5 mm^3) were used in this work. The diamond substrates were rapidly heated to 1050 °C in vacuum (0.1 Pa) with a heating rate of 30 °C/s, keeping at 1050 °C for 0.5, 1, 2, 5, 10, 20, 30 and 60 min, respectively. After that, the samples were cooling to room temperature by immediately turning off the heating source.

2.2. Graphite etching

For hydroxide ion treatment, the surface graphitized diamond sample was fixed onto an anodic platinum electrode by a polytetrafluoroethylene clamp as mentioned in our previous report [13]. The electrodes were dipped in deionized water with a resistivity of 18.25 MΩ cm, and the spacing was about 1 cm. The electric tant was kept at a constant temperature of 25 °C by a cooling device. The hydroxide ion treatments were carried out in deionized water by applying 500 V voltage for 6 h. The current was about 0.1 mA during the hydroxide ion treatments.

2.3. Metal patterning

Gold film with a thickness of 200 nm was patterned on the graphitized diamond surface by electron beam evaporation to form Transmission line model (TLM) configurations. The area was 100 × 100 μm^2, and the spacing was 5, 10, 15, 20, 25 μm, respectively. The uncovered graphite was etched by hydroxide ion treatment. Then, the protective gold film was corroded by I_2:KI (5 %:10 %) solution.

2.4. Raman & XPS characterizations

The Raman spectra were acquired using NTERS-1400R (Tokyo Instruments). The excitation source was a 635 nm laser with a spot size of less than 1 μm and an output power of 3 mW. XPS measurements were performed with a ESCALAB 250Xi (Thermo Fisher). The excitation source of the XPS was Al Kα line with an energy of 1486.6 eV. The X-ray spot size, analyzer pass energy, and the scanning step were 500 μm, 20 eV, and 0.05 eV, respectively. The deconvolution of the spectra was performed by means of XPSPEAK4.1 software.

2.5. AFM & TEM characterizations

Surface morphologies were characterized by a Jiesen SPM-9700HT atomic force microscope (AFM). The graphite/diamond interface structure was studied by TEM (FEI-Talos F200S). The cross-sectional TEM sample was prepared by focus ion beam (FIB) system (Thermo Scientific Helios 5 UX). In order to protect the graphite layer, 100 nm of tungsten was deposited onto the surface.

3. Results and discussion

3.1. Surface graphitization by thermal annealing

After the diamond substrates annealed at 1050 °C under vacuum conditions for varying durations, the surfaces were investigated by Raman spectra as shown in Fig. 1. The Raman spectrum of the original diamond is displayed in Figure S1. The single peak at 1333 cm^{-1} which is related to the first-order Raman line of diamond is evidenced in Fig. 1 (a). However, the G peak of graphite cannot be observed when the sample is annealed for 0.5, 1 or 2 min, possibly owing to the excessively thin graphite layers which is undetectable for Raman spectroscopy.

As annealing time increases to 5 min, the G band of graphite at around 1600 cm^{-1} with very weak intensity emerges in the spectrum. Moreover, the intensity of G band remarkably increases after annealing for 10 min. Meanwhile, a wide band located at 1350 cm^{-1} which is attributed to D peak of sp^2 disordered carbon materials overlaps with the first-order Raman line of diamond, as shown in Fig. 1 (c) [14,15].

As the time for annealing continues to increase, the intensity of both the D band and G band keeps increasing. It indicates that the level of surface graphitization increases with annealing time. However, the sharp tip of the first-order Raman line of diamond still can be observed even after annealing for 60 min. It means that only the surface of diamond is graphitized, making the surface graphite and subsurface diamond simultaneously detectable by Raman spectroscopy.

Since the inelastic mean free path of photoelectrons in bulk materials is just several nanometers, XPS testing is more sensitive to surface information. Therefore, XPS measurements were conducted to study the alterations in surface composition, particularly in the context of brief annealing periods. Fig. 2 displays XPS spectra of the diamond surfaces annealed in vacuum for varying durations. The XPS spectra of the original diamond surface before annealing is displayed in Figure S2.

The backgrounds of all XPS spectra have been corrected with a nonlinear Shirley function. Then, each of the spectra have been fitted with Voigt functions. The predominant components situated at 283.35 and 284.20 eV are related to sp^2 and sp^3 carbon bonds, respectively [16]. It can be observed from Fig. 2 (a) that the sp^2 peak appears when the sample is annealed for 0.5 min, indicating that the diamond surface has been already graphitized. Moreover, the intensities of sp^2 and sp^3 peak are relatively close to each other, suggesting that the graphite layer is extremely thin.

With an increase in annealing time, there is a significant increase in the relative intensity of the sp^2 peak. Meanwhile, the strength of the sp^3 peak decreases apparently. This once again demonstrates that the degree of surface graphitization rises with the duration of annealing. However, the relative intensity of the sp^3 peak remains at a weak strength, as the annealing time increases to 5 ~ 20 min. It may stem from residual sp^3 carbon bonds in the graphite layer, rather than bulk diamond. Therefore, a continuous graphite layer is certainly formed after thermal annealing of 5 min.

The other components with binding energies of 285.10 and 287.02 eV are attributed to C–O and C = O bonds, respectively. When the chamber rapidly heated, adsorbates such as water desorbed and reacted with diamond surface. Therefore, relatively high intensity of C–O peak appears in the XPS spectra after 0.5 min annealing. However, it decreases and keeps at a weak intensity after annealing for 2min. This phenomenon can be explained by the breaking of C–O bonds at 1050 °C, while the amount of desorbed water decreases with annealing time.

Cross-sectional TEM analysis was conducted to further investigate the structural changes of diamond after thermal annealing of 30 min. Fig. 3 (a) - (c) illustrate the various stages involved in the preparation of the cross-sectional TEM lamella. As the surface graphite was rather thin, a 100 nm tungsten layer was deposited onto the surface for protection

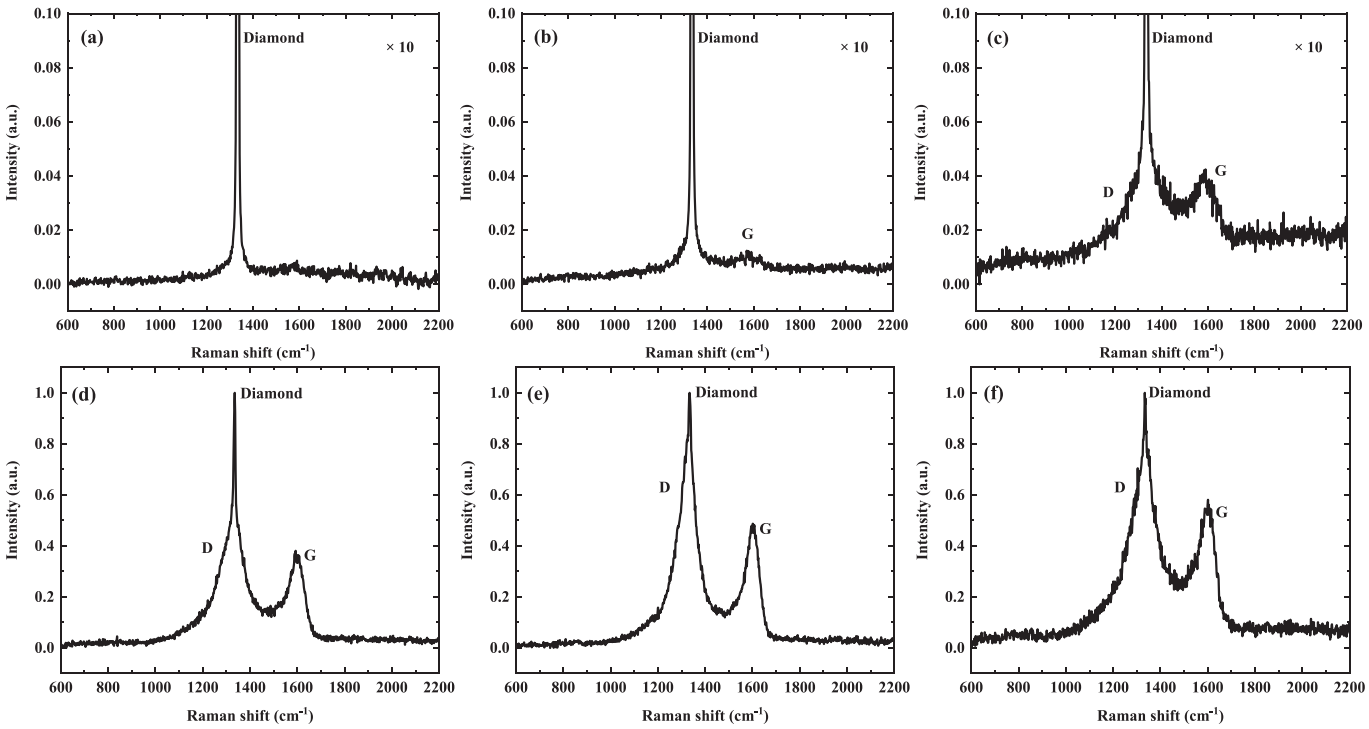

Fig. 1. Raman spectra of diamond surfaces annealed at 1050 °C in vacuum for varying durations: (a) 0.5, 1 or 2 min, (b) 5 min, (c) 10 min, (d) 20 min, (e) 30 min, (f) 60 min.

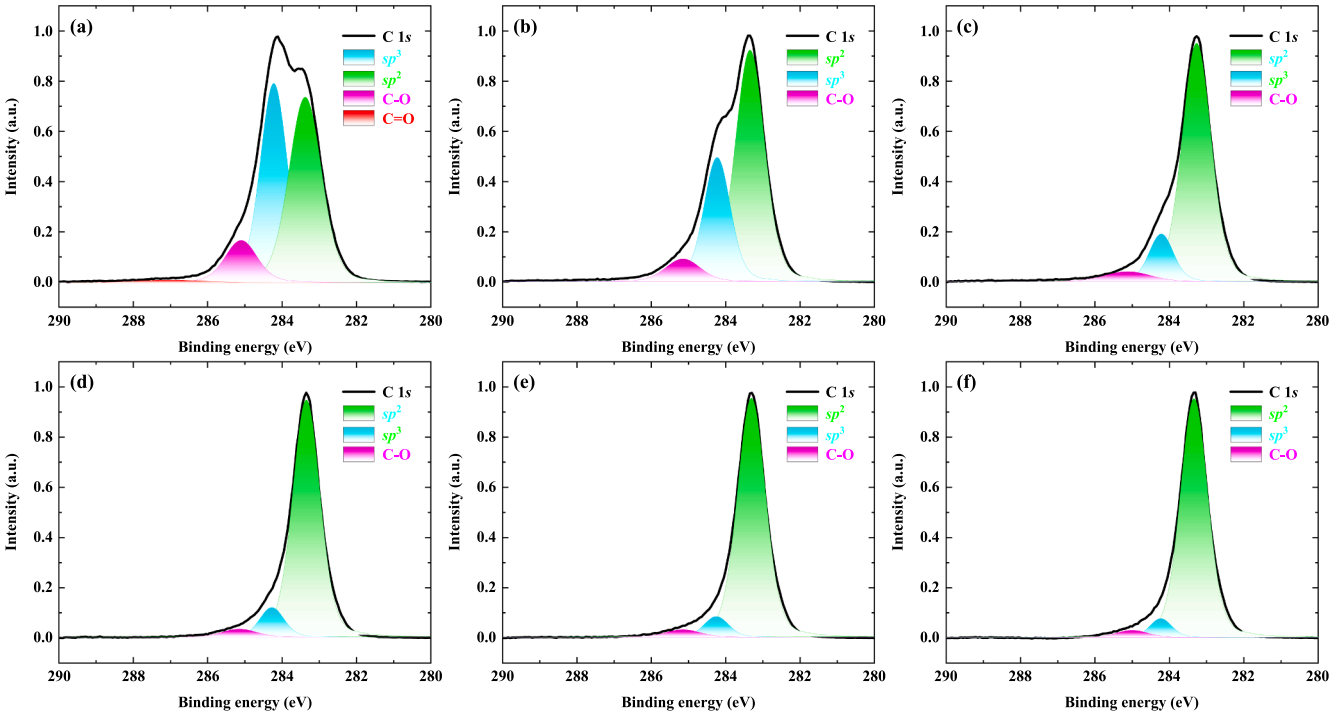

Fig. 2. XPS spectra of the diamond surfaces annealed in vacuum for varying durations: (a) 0.5 min, (b) 1 min, (c) 2 min, (d) 5 min, (e) 10 min, (f) 20 min.

during FIB milling process. Meanwhile, the TEM lamella was flipped so as to thin from diamond to graphite layer for further protection.

The TEM lamella was gradually reduced and polished to approximately 100 nm thickness using FIB. The interface between graphite and diamond is clearly visible in the cross-sectional image, as depicted in Fig. 3 (d). In the diamond region far away from the interface, distinct equidistant planes with an average spacing of 0.206 nm are observed in Fig. 3 (e), which is corresponding to diamond (1 1 1) planes. Meanwhile, the selected area electron diffraction (SAED) exhibits distinct diffraction spots.

Fig. 3 (f) displays the atomic arrangement of the graphite/diamond interface. The diamond region still shows parallel planes spaced at 0.206 nm intervals. However, the SAED shows slightly stretched diffraction spots, suggesting that the crystalline quality of diamond close

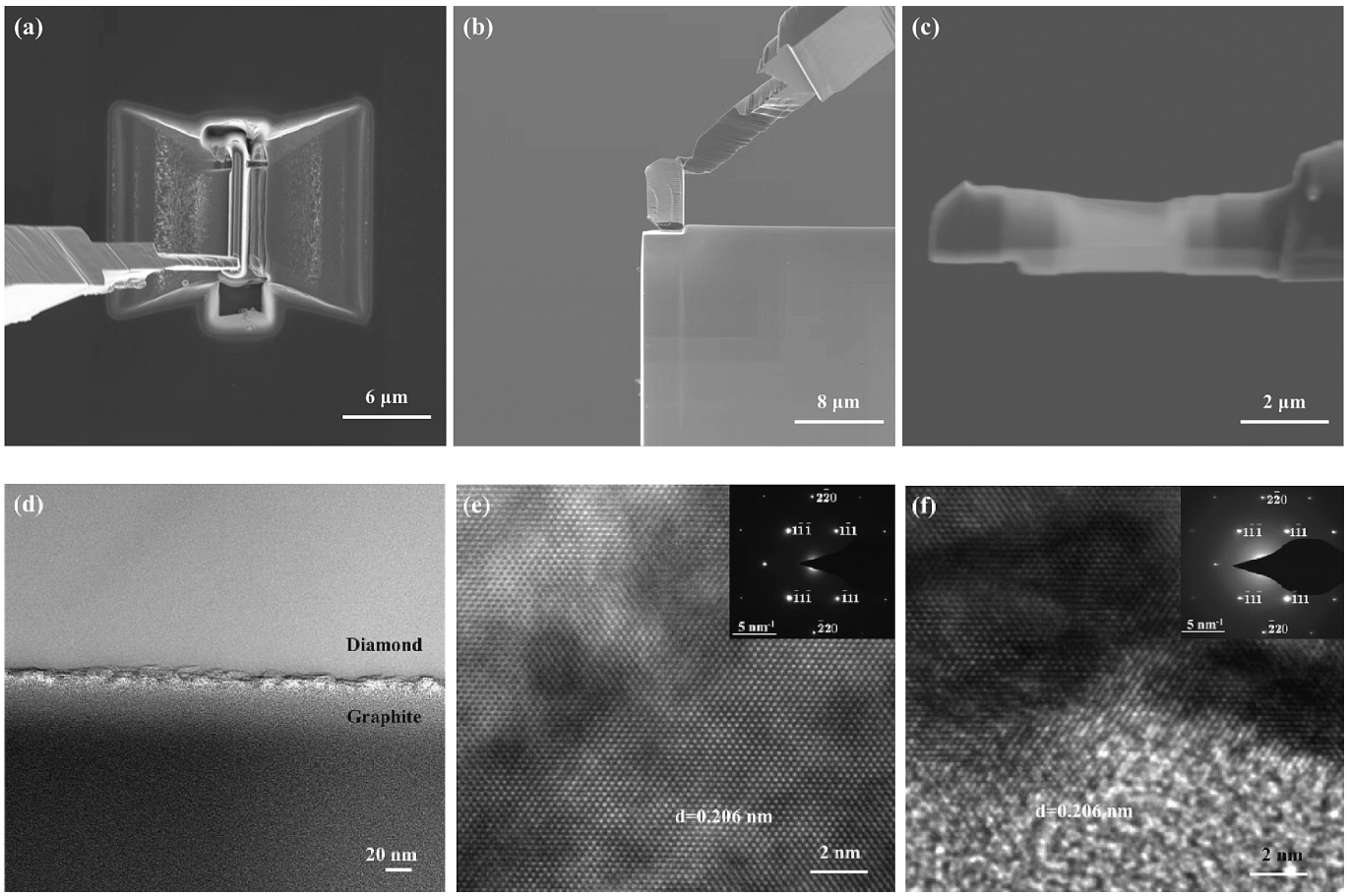

Fig. 3. (a) TEM lamella before extraction; (b) TEM lamella before thinning; (c) TEM lamella after thinning. (d) The cross section of the graphite/diamond; (e) The TEM image of diamond; (f) The TEM image of graphite/diamond interface.

to the interface is comparatively poor. In the bottom region, the crystallographic planes vanish completely. Meanwhile, diffraction rings appear in the inset SAED image. It indicates that nanocrystalline graphite is formed by transforming diamond to graphite during thermal annealing.

3.2. Graphite etching

The diamond substrates were subjected to rapid annealing in vacuum at 1050 °C for 30 min to achieve complete surface graphitization. Then, the sample was processed by hydroxide ion treatment at a high voltage of 500 V in deionized water. Fig. 4 (a) and (b) illustrate AFM images of the diamond surfaces, measuring 1 × 1 μm^2, before and after thermal annealing, respectively. The roughness of the diamond surface decreases after annealing treatment, from 1.86 nm to 1.04 nm (Ra).

As the graphitization gradually extends from surface to subsurface, protrusions are more inclined to be graphitized. These graphitized protrusions are preferentially oxidized by desorbed water, resulting in decrease of surface roughness after thermal annealing. In addition, the surface roughness further decreases to 0.41 nm after hydroxide ion treatment in deionized water for 6 h, as displayed in Fig. 4 (c). This phenomenon can be elucidated by the similar mechanism that graphitized protrusions are completely etched by hydroxide ion treatment.

CVD diamond samples commonly grown in a H_2 (>90 %) and CH_4 atmosphere. The as grown diamond surface is typically terminated by hydrogen atoms, which has a p-type surface conductivity induced by two-dimensional hole gases. Fig. 5 (a) exhibits the XPS spectrum of the as grown diamond. The dominant component with a binding energy of

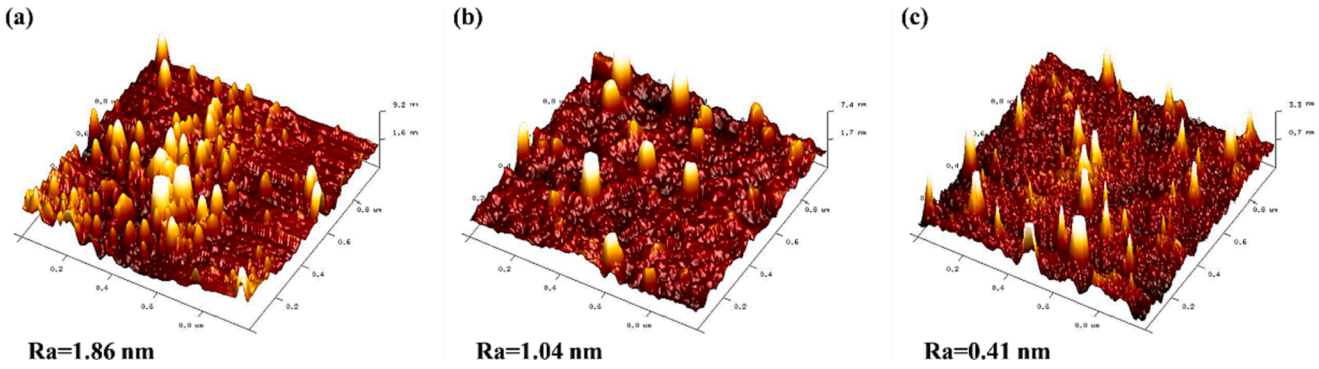

Fig. 4. AFM images of the diamond surfaces: (a) as grown diamond, (b) after thermal annealing, (c) after hydroxide ion treatment.

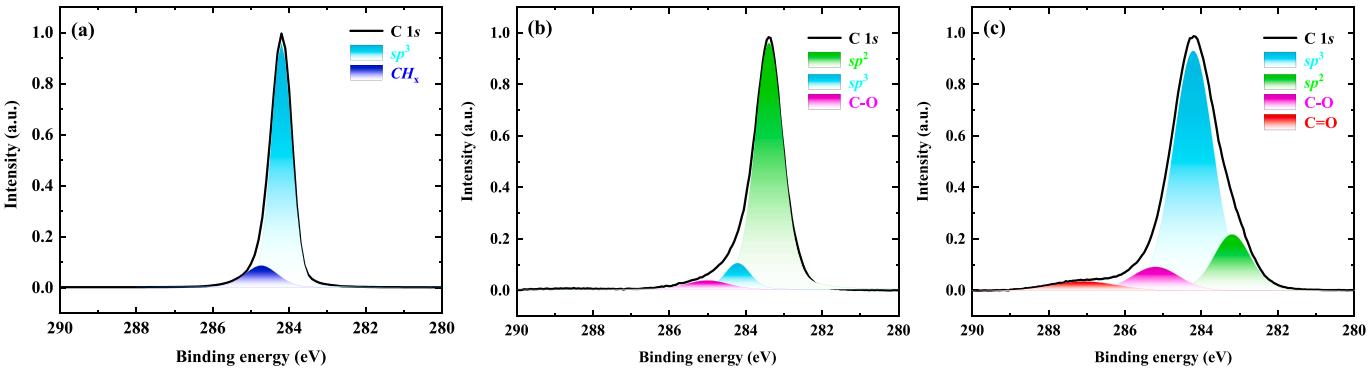

Fig. 5. XPS spectra of the diamond surfaces: (a) as grown diamond, (b) after thermal annealing, (c) after hydroxide ion treatment.

284.20 eV is attributed to bulk sp^3 carbon bonds. The secondary component can be assigned to CH_x groups, resulting from carbon-hydrogen bonds in the diamond surface generated during CVD growth [17].

After thermal annealing at 1050 °C in vacuum, the sp^3 carbon bonds transform to sp^2 carbon bonds, as shown in the Fig. 5 (b). Meanwhile, the full width at half maximum (FWHM) increases from 0.67 eV to 0.84 eV, indicating deterioration of surface after graphitization. Moreover, the CH_x groups disappear in the XPS spectrum. It suggests that CH_x bonds are desorbed by thermal annealing [18]. In addition, C-O peak appears in the spectrum, which stems from diamond surface oxidation with the adsorbates in the chamber during annealing.

Fig. 5 (c) illustrates the XPS spectrum of the graphitized diamond surface processed by hydroxide ion treatment in deionized water at high voltage. The dominant component is again attributed to sp^3 carbon bonds, suggesting that the surface graphite was etched to reveal the diamond after hydroxide ion treatment. Meanwhile, the relative intensity of sp^2 carbon bonds apparently decreases. These observations indicate that graphite has been successfully etched by hydroxide ions.

The residual sp^2 carbon bonds should stem from surface reconstruction during oxidation by hydroxide ions. The phenomenon has also been observed for diamond surfaces after traditional oxidation methods, such as vacuum ultraviolet ozone and chemical acid treatments [16]. The intensity ratio of sp^2 peak to sp^3 peak is only about 0.21, which is a relatively low value.

For comparison, the graphitized surface is also etched by argon ion etching, as shown in the Supplementary Material. The surface roughness increases to 2.32 nm after 1000 eV argon ion etching, which is 0.41 nm for the hydroxide ion treated surface. Moreover, the intensity ratio of sp^2 peak to sp^3 peak is about 1.24 for argon ion etched diamond surface, which is 0.21 for the hydroxide ion treated surface. By contrast, the level of damage caused by hydroxide ion treatment is significantly lower.

3.3. Selective etching and TLM measurements

The diamond surfaces were graphitized by thermal annealing in vacuum at 1050 °C in vacuum for 10, 30 and 60 min, respectively. Then, 200 nm gold patterns were fabricated on the substrate via photolithography and electron beam evaporation. In order to enhance the adhesion between gold and graphite, the sample was further annealed in vacuum at 600 °C in vacuum for 1 h. After that, the sample was processed by hydroxide ion treatment, resulting in corrosion of uncovered graphite. Then, the protective gold film was corroded by I_2:KI (5 %:10 %) solution.

In Fig. 6, the thickness of surface graphite resulting from vacuum annealing of diamond for different durations is presented. The graphite thickness is about 35 nm for 10 min annealing, 108 nm for 30 min annealing, and 202 nm for 60 min annealing. Therefore, the growth rate of graphite thickness induced by vacuum annealing at 1050 °C is approximately 3.3 ~ 3.6 nm per minute. It should be mentioned that the rate of graphite layer formation by thermal annealing could be different in the early stages, which may be relative lower in the beginning.

For TLM measurement, boron-doped (~10^{20} cm^{-3}) diamond substrates are used. TLM patterns were formed on the graphitized diamond surface by electron beam evaporation, as shown in Fig. 7 (a). The gold square is 100 × 100 μm^2, and the spacing is 5, 10, 15, 20, 25 μm, respectively. The uncovered graphite and the protective gold were successively etched by hydroxide ion treatment and I_2:KI solution, respectively. Raman mapping of 50 × 50 μm^2 were conducted after hydroxide ion treatment and after I_2:KI solution processing.

Fig. 7 (b) exhibits the Raman mapping of the sample surface after hydroxide ion treatment. The uncovered graphite is completely etched away during hydroxide ion treatment, exposing the diamond surface. Meanwhile, the gold square is not affected by the high-voltage processing. After dissolving the gold protective layer, the underlying graphite is revealed, as illustrated by Fig. 7 (c). It can be observed that

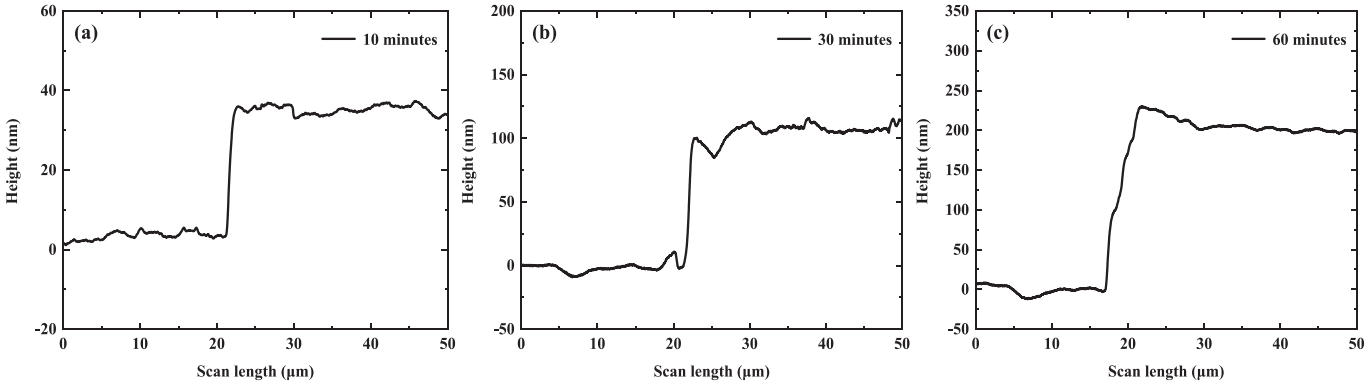

Fig. 6. The thickness of surface graphite formed by annealing diamond in vacuum for varying durations: (a) 10 min, (b) 30 min, (c) 60 min.

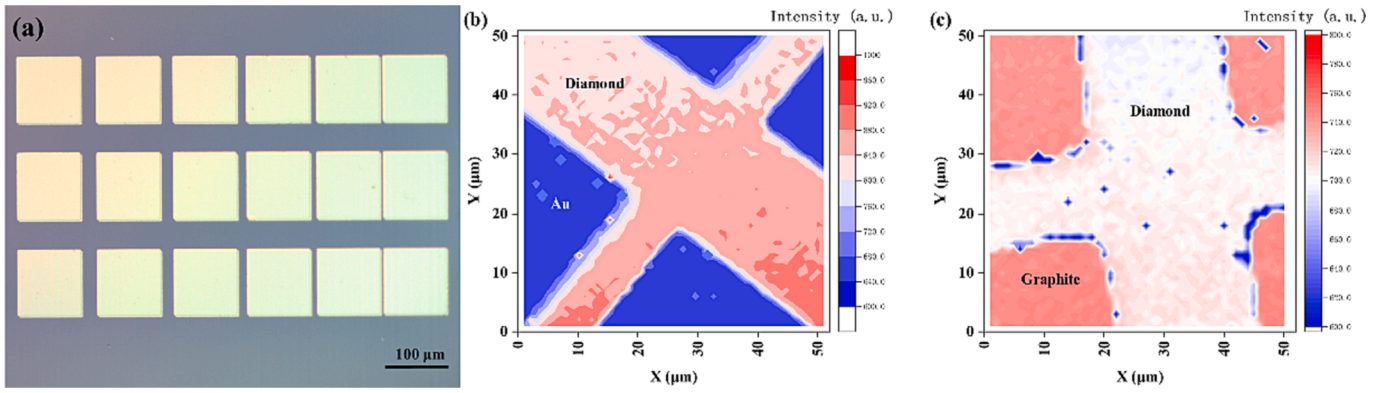

Fig. 7. (a) Optical image of the graphitized diamond surface with gold patterns, (b) Raman mapping after hydroxide ion treatment, (c) Raman mapping after I_2: KI corrosion.

the graphite pattern maintains its shape after selectively etching.

Current-voltage (I-V) characteristics of adjacent graphite electrodes with varying separation distances are presented in Fig. 8 (a). Notably, the I-V curves exhibit an almost linear trend, indicative of ohmic contact formation at the graphite/diamond interface. The total resistance R_T between two adjacent graphite electrodes can be accurately calculated using the following equation as reported in reference [19]:

$$R_T = \frac{R_s}{Z}d + \frac{2R_sL_T}{Z} \quad (1)$$

The parameter "Rs" in the equation represents the sheet resistance of the diamond substrate, "d" denotes the spacing of electrodes, "Z" signifies the length of the graphite electrodes, and "L_T" corresponds to the transfer length. As a result, the specific contact resistance can be computed by applying the subsequent formula:

$$\rho_c = R_sL_T^2 \quad (2)$$

The R_s and L_T parameters can be derived through linear regression analysis of R_T as a function of spacing d, as illustrated in Fig. 8 (b). Subsequently, the specific contact resistance ρ_c of the graphite/diamond contact is determined to 2.53×10^{-4} Ω cm^2. The value is lower than the graphite/diamond contact induced by laser irradiation, which is about 7.83×10^{-5} Ω cm^2 [20]. Probably, it is due to a better transition interface of the laser induced graphite/diamond contact.

4. Conclusions

In summary, surface graphitization of diamond is achieved through rapid thermal annealing at 1050 °C in a vacuum environment. The thickness of graphite layers formed by thermal annealing is approximately 3.3 ~ 3.6 nm per minute. As the graphite thickness is likely to be several nanometers with annealing durations of less than 2 min, sp^2 and sp^3 carbon bonds are simultaneously detected by XPS. Whereas, the sp^3 carbon bonds can be no longer perceived after prolonged annealing, when the graphite layer is thick enough to impede the escape of diamond photoelectrons. In contrast, the information of sp^2 carbon bonds for short-time annealed samples is difficult to be acquired by Raman spectra. The G peak is absent in Raman spectra for diamond samples annealed less than 2 min, due to thin graphite layers. However, both the G peak and D band are observed in the Raman spectra after annealing for 10 min, and continue to increase in intensity as the annealing duration is extended.

A distinct atomic interface between graphite and diamond is observed via cross-sectional transmission electron microscopy. According to the slightly stretched diffraction spots from SAED, the crystalline quality of diamond close to the interface is comparatively poor. Then, hydroxide ion treatment is used to remove the surface graphite, resulting in reduced roughness and fewer damages based on the AFM and XPS results. In the end, the graphite/diamond contact with TLM patterns is fabricated by selective etching via hydroxide ion treatments. The uncovered graphite is completely etched away during high-voltage processing, while the graphite protected by gold patterns is not affected.

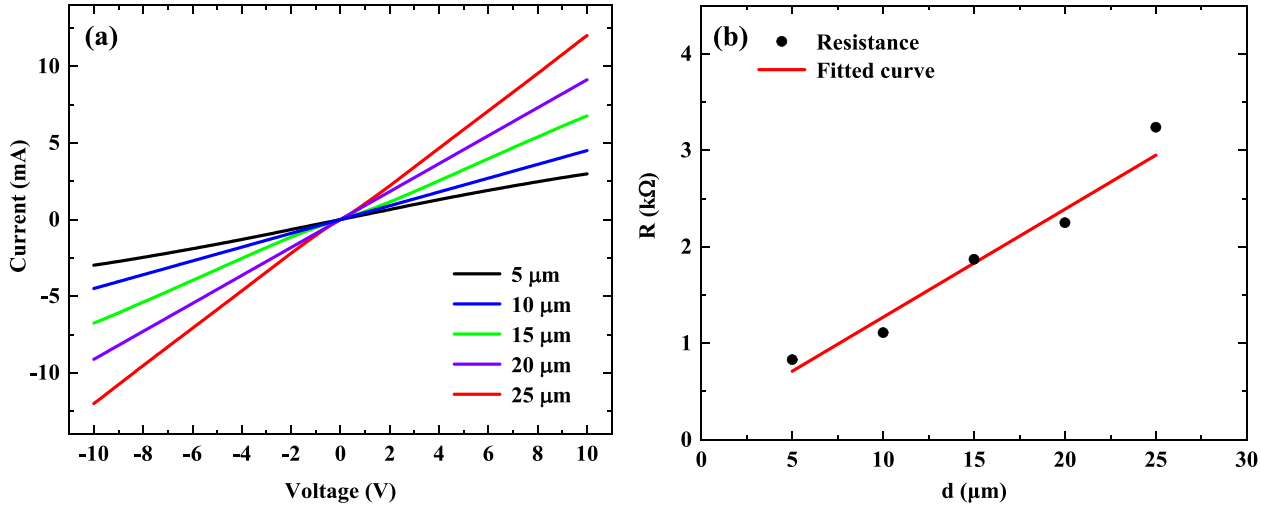

Fig. 8. (a) I-V characteristics of adjacent graphite electrodes with different spacing, (b) dependence of R on d for the graphite/diamond contacts.

The specific contact resistance of the graphite/diamond contact is determined to be 2.53×10^{-4} Ω cm^2

CRediT authorship contribution statement

F.N. Li: Writing – review & editing, Writing – original draft, Investigation, Funding acquisition, Formal analysis, Data curation, Conceptualization. **P.C. Zhang:** Investigation. **P.F. Zhang:** Investigation. **H.X. Wang:** Supervision, Funding acquisition.

Declaration of competing interest

The authors declare that they have no known competing financial interests or personal relationships that could have appeared to influence the work reported in this paper.

Data availability

Data will be made available on request.

Acknowledgment

This work was supported by National Natural Science Foundation of China (Grant No.62104189), China Postdoctoral Science Foundation (Grant No.2020 M683483) and Natural Science Foundation of Shannxi Province, China (Grant No. 2022JM-008). We thank C.Y. Liang at Instrument Analysis Center of Xi'an Jiaotong University for her assistance with XPS analysis.

Appendix A. Supplementary data

Supplementary data to this article can be found online at https://doi.org/10.1016/j.apsusc.2024.159753.

References

[1] C.Q. Dang, J.P. Chou, B. Dai, C.T. Chou, Y. Yang, R. Fan, W.T. Lin, F.L. Meng, A. Hu, J.Q. Zhu, J.C. Han, A.M. Minor, J. Li, Y. Lu, Achieving large uniform tensile elasticity in microfabricated diamond, Sci. 371 (2021) 76–78.
[2] S.A. Manifold, G. Klemencic, E.L.H. Thomas, S. Mandal, H. Bland, S.R. Giblin, O. A. Williams, Contact resistance of various metallisation schemes to superconducting boron doped diamond between 1.9 and 300 K, Carbon. 179 (2021) 13e19.
[3] P. Hazdra, A. Laposa, Z. Soban, J. Voves, N. Lambert, M. Davydova, V. Povolný, A. Taylor, V. Mortet, Low-resistance ohmic contacts on boron-doped 113 oriented homoepitaxial diamond layers, Dia. Relat. Mater. 121 (2022) 108797.
[4] Y.Q. Ma, B.L. Liu, A.Y. Zhang, L. Chen, M. Fathi, C.F. Shen, A.N. Abbas, M.Y. Ge, M. Mecklenburg, C.W. Zhou, Reversible semiconducting-to-metallic phase transition in chemical vapor deposition grown monolayer WSe_2 and applications for devices, ACS Nano. 9 (2015) 7383–7391.
[5] H.J. Yang, S.W. Kim, M. Chhowalla, Y.H. Lee, Structural and quantum-state phase transitions in van der Waals layered materials, Nat. Phys. 13 (2017) 931–938.
[6] P. Yu, J.H. Lin, L.F. Sun, Q.L. Le, X.H. Yu, G.H. Gao, C.H. Hsu, D. Wu, T.R. Chang, Q.S. Zeng, F.C. Liu, Q.J. Wang, H.T. Jeng, H. Lin, A. Trampert, Z.X. Shen, K. Suenaga, Z. Liu, Metal–semiconductor phase-transition in WSe2(1–x)Te2x monolayer, Adv. Mater. 29 (2017) 1603991.
[7] M. Komlenok, A. Bolshakov, V. Ralchenko, V. Konov, G. Conte, M. Girolami, P. Oliva, S. Salvatori, Diamond detectors with laser induced surface graphite electrodes, Nucl. Inst. Methods Phys. Res. A 837 (2016) 136–142.
[8] M. Pacilli, P. Allegrini, M. Girolami, G. Conte, E. Spiriti, V.G. Ralchenko, M. S. Komlenok, A.A. Khomic, V.I. Konov, Polycrystalline CVD diamond pixel array detector for nuclear particles monitoring, J. Instrum. 8 (2013) C02043.
[9] X.B. Yan, J.J. Wei, K. An, J.L. Liu, L.X. Chen, X.T. Zhang, C.M. Li, Graphitization of CVD diamond grain boundaries during transient heat treatment, Dia. Relat. Mater. 116 (2021) 108433.
[10] L. Nisto, V. Ralchenko, I. Vlasov, A. Khomich, R. Khmelnitskii, P. Potapov, J. V. Landuyt, Formation of amorphous carbon and graphite in CVD diamond upon annealing: A HREM, EELS, Raman and Optical Study, Phys. Stat. Sol. A. 186 (2001) 207–214.
[11] V. Ralchenko, L. Nistor, E. Pleuler, A. Khomich, I. Vlasov, R. Khmelnitskii, Structure and properties of high-temperature annealed CVD diamond, Dia. Relat. Mater. 12 (2003) 1964–1970.
[12] F.N. Li, Y. Li, D.Y. Fan, H.X. Wang, Barrier heights of Au, Pt, Pd, Ir, Cu on nitrogen terminated (1 0 0) diamond determined by X-ray photoelectron spectroscopy, Appl. Surf. Sci. 456 (2018) 532–537.
[13] F.N. Li, Y. Li, H.W. Bao, H.X. Wang, F. Ma, Fabrication of hydroxyl terminated diamond by high-voltage hydroxide ion treatments, Appl. Surf. Sci. 622 (2023) 156909.
[14] J. Schwan, S. Ulrich, V. Batori, H. Ehrhardt, S.R.P. Silva, Raman spectroscopy on amorphous carbon films, J. Appl. Phys. 80 (1996) 440–447.
[15] M.J. Matthews, M.A. Pimenta, G. Dresselhaus, M.S. Dresselhaus, M. Endo, Origin of dispersive effects of the Raman D band in carbon materials, Phys. Rev. B. 59 (1999) R6585–R6588.
[16] F.N. Li, R. Akhvlediani, M.K. Kuntumalla, A. Hoffman, Oxygen bonding configurations and defects on differently oxidized diamond surfaces studied by high resolution electron energy loss spectroscopy and X-ray photoelectron spectroscopy measurements, Appl. Surf. Sci. 465 (2019) 313–319.
[17] S. Kono T. Saito S.H. Kang W.Y. Jung B.Y. Kim H. kawata, T. Goto, Y. Kakefuda, H. W. Yeom Band diagram for chemical vapor deposition diamond surface conductive layer: Presence of downward band bending due to shallow acceptors Surf. Sci. 604 2010 1148 1165.
[18] J.B. Cui, J. Ristein, L. Ley, Electron affinity of the bare and hydrogen covered single crystal diamond (111) surface, Phys. Rev. Lett. 81 (1998) 429.
[19] C.M. Zhen, X.Q. Wang, X.C. Wu, C.X. Liu, D.L. Hou, Au/p-diamond ohmic contacts deposited by RF sputtering, Appl. Surf. Sci. 255 (2008) 2916–2919.
[20] F.N. Li, H.W. Bao, Y. Li, F. Ma, H.X. Wang, Laser induced diamond/graphite structure for all-carbon deep-ultraviolet photodetector, Appl. Surf. Sci. 636 (2023) 157818.